Quantification of porosity and deposition rate of nanoporous films grown by oblique-angle deposition

D. J. Poxson,[1] F. W. Mont,[2] M. F. Schubert,[2] J. K. Kim,[2] and E. F. Schubert[1,2,a)]
[1]*Future Chips Constellation, Department of Physics, Applied Physics, and Astronomy, Rensselaer Polytechnic Institute, Troy, New York 12180, USA*
[2]*Future Chips Constellation, Department of Electrical, Computer, and Systems Engineering, Rensselaer Polytechnic Institute, Troy, New York 12180, USA*

(Received 2 July 2008; accepted 25 August 2008; published online 11 September 2008)

We propose an analytic model that accurately predicts the porosity and deposition rate of nanoporous films grown by oblique-angle deposition. The model employs a single fitting parameter and takes into account geometrical factors as well as surface diffusion. We have determined the porosity and deposition rate from the measured refractive index and thickness of SiO_2 and indium tin oxide nanoporous films deposited at various incident angles. Comparison of experimental data with the model reveals excellent agreement. The theoretical model allows for the predictive control of refractive index, porosity, and deposition rate for a wide range of deposition angles and materials. © *2008 American Institute of Physics*. [DOI: 10.1063/1.2981690]

In the optical sciences, the refractive index of a medium is the most fundamental quantity. Yet optical thin film materials with very low refractive indices, close to that of air, had been unavailable until recently when a new class of high-quality, low-refractive-index (low-*n*) materials was demonstrated through the use of oblique-angle deposition of SiO_2 and indium tin oxide (ITO).[1,2] Using this technique, the accurate control of the refractive index of *any* physical-vapor deposited thin film material can be achieved. By controlling the refractive index in multilayer graded-index films, it was shown that Fresnel reflection can be virtually eliminated.[1,3] Such low-*n* films, and their index controllability, are highly desirable for a variety of optical applications, for example, broadband antireflection coatings,[4–6] omnidirectional reflectors,[7,8] distributed Bragg reflectors,[9,10] optical microresonators,[11] light-emitting diodes,[12] photovoltaic solar cells,[13] and optical interconnects.[14] In oblique-angle deposition, first demonstrated in 1886,[15] the growth and tunability of low-*n* films is achieved by control of the vapor flux incident angle.[1] For low-*n* films, two important characteristics exist: the refractive index and thickness of the film. Formulas accurately predicting these values, for a given vapor flux incident angle, are highly desirable. The qualitative tenets of oblique-angle deposition were laid out over a century ago, and there have been a number of studies on the structure of obliquely deposited thin films. Relations between incident vapor flux angle and column orientation have been proposed.[16,17] More recently, expressions describing column angle and density as a function of deposition angle for films evaporated under conditions allowing only limited surface diffusion have been reported.[18]

In this publication, we propose a model relating the porosity and deposition rate of a material to its vapor flux incidence angle for oblique-angle deposition. Our model, which employs a single fitting parameter, *c*, is based upon geometrical arguments, and takes into account surface diffusion. Porosity and deposition rates directly relate to the refractive index and thickness, respectively, and therefore such formulas allow for a predictive control of nanoporous film deposition, a capability that is highly relevant for the application of low-*n* materials.

The porosity of a thin film, *P*, is defined as the ratio between the volume of air in the film, V_{air}, to the total volume of the film, V_{film}. V_{film} is the sum of the volume of the deposited materials in the film, $V_{material}$, plus the volume of air V_{air},

$$P = \frac{V_{air}}{V_{film}} = \frac{V_{air}}{V_{material} + V_{air}}. \quad (1)$$

Next, an expression for V_{air} is derived using geometrical arguments. A schematic of the oblique-angle deposition process is shown in Fig. 1. Let us assume that the incident vapor flux forms nucleation sites or islands of height *h*. These islands prevent the incident vapor flux from reaching the region where deposition is obstructed. The shadow length, *s*, is given by $h \tan \theta$, where each nanocolumn is considered independent from one another. It is this self-shadowing that gives rise to a self-organized nanocolumnar growth. Incident vapor flux preferentially deposits on top of these nanocolumns which then begin to grow at a non-normal angle, however column angle is neglected in these calculations. As the

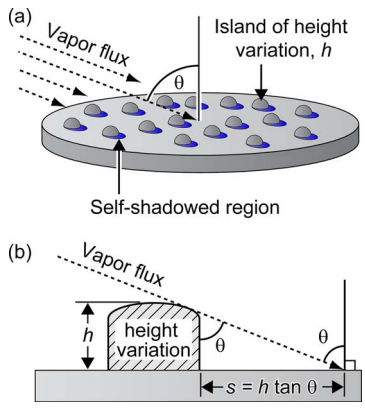

FIG. 1. (Color online) Incident vapor flux of angle θ, strikes height variation *h* thereby forming a shadow region *s*.

a)Electronic mail: efschubert@rpi.edu.

height and volume of these columns increase, so does the volume of the shadowed volume, given by $A_{cs}s$, where A_{cs} is the cross-sectional area of the nanocolumn, considered independent of θ. By using the expressions for the shadow length and air volume, we obtain the porosity as

$$P = \frac{A_{cs}h \tan\theta}{V_{material} + A_{cs}h \tan\theta}, \tag{2}$$

where $V_{material}$ is the volume of a nanocolumn. The following intuitive boundary conditions are satisfied by Eq. (2), at normal incidence, $\theta=0°$, a nonporous film is obtained, that is, $P=0\%$, while at $\theta=90°$, the porosity is given by $P=100\%$.

Next, we take into account surface diffusion during the oblique-angle deposition process. At very small angles θ, a nonzero, finite shadow length is predicted by $s=h\tan\theta$. However, it is intuitively clear that surface diffusion of atoms will prevent the formation of a shadow region for extremely small shadow lengths, i.e., for very small angles θ. This property can be expressed as $ds=0$ for $\theta\approx0°$ or $ds/d\theta|_{\theta°=0}=0$. On the contrary, for large values of s, i.e., for θ approaching 90°, the shadow length should be unaffected by surface diffusion because the shadow length is much greater than the diffusion length. Alternatively, from a mathematical and symmetry perspective, we postulate that the function $s(\theta)$ and its derivative must be continuous functions at $\theta=0°$ i.e., $ds/d\theta|_{\theta=0}=0$. We therefore write the shadow length as $s=f(\theta)h\tan\theta$, where $f(\theta)$ is a function yet to be determined by the above-mentioned boundary condition

$$\left.\frac{ds}{d\theta}\right|_{\theta=0} = 0. \tag{3}$$

Besides the trivial solution $f(\theta)=0$, the simple function $f(\theta)=\theta/(\pi/2)$ satisfies this boundary condition. This function ensures that due to surface diffusion, no shadows form near $\theta=0°$ and that diffusion has a negligible effect on the shadow length for angles near 90°. This result used together with Eqs. (1) and (2), yields

$$P = \frac{\theta\tan\theta}{c+\theta\tan\theta}, \quad \text{where } c = \frac{\pi V_{material}}{2A_{cs}h}. \tag{4}$$

With this expression we are able to compare experimental data to the theoretical prediction made by Eq. (4). We acquired experimental data for obliquely deposited nanoporous films of SiO_2 and ITO. The materials were deposited on a silicon substrate using an electron-beam deposition system. Thickness and deposition rate were monitored using a quartz crystal sensor. The deposition rate was manually controlled at a constant rate of 0.2 nm s^{-1} and deposition was terminated when the quartz crystal monitor measured 200 nm. Sample thickness and refractive index were then measured using ellipsometery. The porosity of these thin films is then determined from the refractive index based on the linear volume approximation,[19] the Bruggeman effective medium approximation did not yield an appreciable difference.[20] Figure 2 shows the porosity of nanoporous films of SiO_2 and ITO deposited by oblique-angle deposition for a variety of angles and the theoretical curve of Eq. (4) using $c=3.17$ for SiO_2 and $c=3.55$ for ITO. Experimental data and the proposed theoretical model are in excellent agreement with a correlation coefficient $R^2>99\%$ for both data sets.

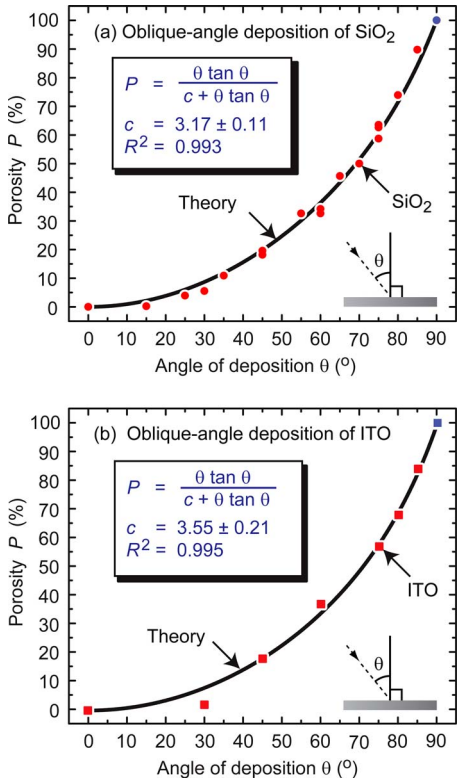

FIG. 2. (Color online) Theoretical model of porosity vs angle plotted with experimentally measured porosity data for (a) SiO_2, and (b) ITO nanoporous films.

We proceed to calculate the deposition rate of a nanoporous, oblique-angle deposited films. First, we describe the deposition rate of a film grown at normal incidence as

$$GR_{\perp} = F, \tag{5}$$

where F is the volume flux of incident material ($cm^3\,cm^{-2}\,s^{-1}$). Tilting the substrate by an angle θ changes the projected area by a factor of $\cos\theta$. Therefore, the deposition rate at such an oblique incidence is

$$GR_{\angle} = F\cos\theta. \tag{6}$$

The deposition rate of a nanoporous film can now be expressed in terms of the volume flux and the porosity P as

$$GR_{\angle} = \frac{F\cos\theta}{1-P} = \frac{F\cos\theta}{1-\dfrac{\theta\tan\theta}{c+\theta\tan\theta}}, \tag{7}$$

where Eq. (4) was used to eliminate the porosity.

The normalized deposition rate GR_n is found by dividing Eq. (7) by the deposition rate at normal incidence

$$GR_n = \frac{GR_{\angle}(\theta)}{GR_{\angle}(\theta=0)}. \tag{8}$$

Next we compare the experimental deposition rate with the theoretical expression for the normalized deposition rate. Each SiO_2 and ITO data point was normalized by dividing measured thickness for a given angle θ by the thickness (318 and 200 nm, respectively) at normal incidence ($\theta=0°$), as measured by ellipsometry. Figure 3 plots the normalized deposition rates using the corresponding c values for SiO_2 and ITO along with the theoretical curves. Inspection of Fig.

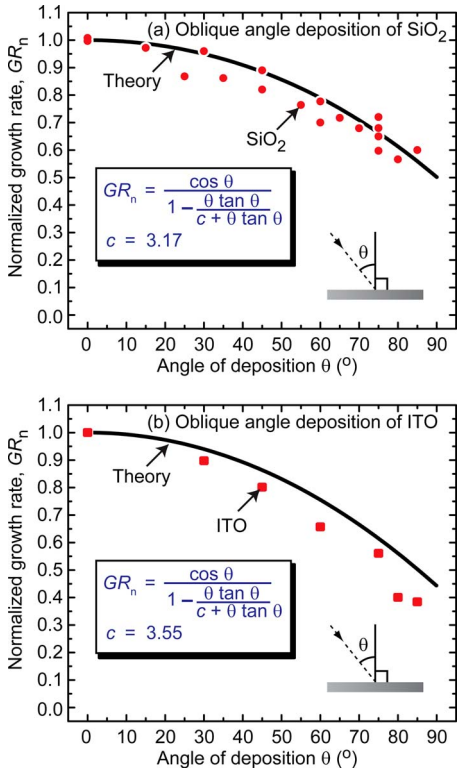

FIG. 3. (Color online) Experimental deposition rate of (a) SiO_2 and (b) ITO nanoporous films, plotted with theoretical equation for deposition rate.

3 shows excellent agreement between experimental and theoretical deposition rates. Of particular interest are the deposition rates at incident angles close to 90°; we note that in the limit $\theta \rightarrow 90°$, the calculated deposition rate for SiO_2 tends toward 0.50 and deposition rate for ITO tends toward 0.44, both in excellent agreement with experiment.

In summary, we have presented a detailed quantitative analysis of the porosity and deposition rate of nanoporous thin films deposited by oblique-angle evaporation. We have measured the thickness and refractive index for SiO_2 and ITO nanoporous films deposited over a wide range of deposition angles. The porosity of a material was determined from the measured refractive index. We have developed a theoretical model for porosity and deposition rate of obliquely deposited thin films while considering the formation of shadow regions and surface diffusion effect. Comparison of experimental data with the proposed theoretical model reveals excellent agreement. The theoretical model allows for the predictive control of porosity and deposition rate for all deposition angles, potentially a very useful tool in the development of high-quality low-*n* optical coatings. Furthermore, given the set of basic assumptions used, we expect these formulas to be valid for a wide range of materials.

The authors gratefully support through the Nanoscale Science and Engineering Center for Directed Assembly of Nanostructures directed by Richard W. Siegel. The authors also gratefully acknowledge support from Sandia National Laboratories, DOD, DOE, NSF, Crystal IS, Magnolia Optics, Samsung Electro-Mechanics Company, Troy Research Corporation, and NY State.

[1] J.-Q. Xi, M. F. Schubert, J. K. Kim, E. F. Schubert, M. Chen, S.-Y. Lin, W. Liu, and J. A. Smart, Nat. Photonics **1**, 176 (2007).
[2] J. K. Kim, S. Chhajed, M. F. Schubert, E. F. Schubert, A. J. Fischer, M. H. Crawford, J. Cho, H. Kim, and C. Sone, Adv. Mater. (Weinheim, Ger.) **20**, 801 (2008).
[3] J.-Q. Xi, J. K. Kim, and E. F. Schubert, Nano Lett. **5**, 1385 (2005).
[4] W. H. Southwell, Opt. Lett. **8**, 584 (1983).
[5] J. A. Dobrowolski, D. Poitras, P. Ma, H. Vakil, and M. Acree, Appl. Opt. **41**, 3075 (2002).
[6] D. Poitras and J. A. Dobrowolski, Appl. Opt. **43**, 1286 (2004).
[7] J.-Q. Xi, M. Ojha, J. L. Plawsky, W. N. Gill, J. K. Kim, and E. F. Schubert, Appl. Phys. Lett. **87**, 031111 (2005).
[8] J.-Q. Xi, M. Ojha, J. L. Plawsky, W. N. Gill, Th. Gessmann, and E. F. Schubert, Opt. Lett. **30**, 1518 (2005).
[9] R. Sharma, E. D. Haberer, C. Meier, E. L. Hu, and S. Nakamura, Appl. Phys. Lett. **87**, 051107 (2005).
[10] M. H. MacDougal, H. Zhao, P. D. Dapkus, M. Ziari, and W. H. Steier, Appl. Phys. Lett. **57**, 1387 (1990).
[11] Q. Xu, V. R. Almeida, R. R. Panepucci, and M. Lipson, Opt. Lett. **29**, 1626 (2004).
[12] J. K. Kim, J.-Q. Xi, H. Luo, J. Cho, C. Sone, Y. Park, Th. Gessmann, and E. F. Schubert, Appl. Phys. Lett. **88**, 013501 (2006).
[13] J. Zhao and M. A. Green, IEEE Trans. Electron Devices **38**, 1925 (1991).
[14] A. Jain, S. Rogojevic, S. Ponoth, N. Agarwal, I. Matthew, W. N. Gill, P. Persans, M. Tomozawa, J. L. Plawsky, and E. Simonyi, Thin Solid Films **398**, 513 (2001).
[15] A. Kundt, Ann. Phys. Chem. **27**, 59 (1886).
[16] J. M. Nieuwenhuizen and H. B. Haanstra, Philips Tech. Rev. **27**, 87 (1966).
[17] S. Lichter and J. Chen, Phys. Rev. Lett. **56**, 1396 (1986).
[18] R. N. Tait, T. Smy, and M. J. Brett, Thin Solid Films **226**, 196 (1993).
[19] W. H. Southwell, Appl. Opt. **24**, 457 (1985).
[20] P. K. H. Ho, D. S. Thomas, R. H. Friend, and N. Tessler, Science **285**, 233 (1999).